GLOBAL JOURNAL OF ENGINEERING, DESIGN & TECHNOLOGY
(Published By: Global Institute for Research & Education)
www.gifre.org

THE EFFECTS OF THERMAL RADIATION, HEAT GENERATION, VISCOUS DISSIPATION AND CHEMICAL REACTION ON MHD MICROPOLAR FLUID PAST A STRETCHING SURFACE IN A NON-DARCIAN POROUS MEDIUM

B. Lavanya[1] & A. Leela Ratnam[2]

[1]Department of Mathematics, Priyadarshini College of Engineering & Technology, Nellore.
[2]Department of Applied Mathematics, Sri Padmavathi Mahila Visva Vidyalayam, Tirupathi.

Abstract

The main concern of present study is to investigate the effects of thermal radiation and chemical reaction on a steady two-dimensional laminar flow of a viscous incompressible electrically conducting micropolar fluid past a vertical isothermal stretching surface embedded in a non-Darcian porous medium in the presence of viscous dissipation and heat generation. The governing equations of momentum, angular momentum, energy, and species equations are solved numerically using Runge-Kutta fourth order method with the shooting technique. The effects of various parameters on the velocity, microrotation, temperature and concentration field as well as skin friction coefficient, Nusselt number and Sherwood number are shown graphically and tabulated. It is observed that the micropolar fluid helps in the reduction of drag forces and also acts as a cooling agent. An excellent agreement is observed between some of the obtained results of the current study and those of previously published studies.

Introduction

The free convection processes involving the combined mechanism of heat and mass transfer are encountered in many natural processes, in many industrial applications and in many chemical processing systems. The study of free convective mass transfer flow has become the object of extensive research as the effects of heat transfer along with mass transfer effects are dominant features in many engineering applications such as rocket nozzles, cooling of nuclear reactors, high sinks in turbine blades, high speed aircrafts and their atmospheric re-entry, chemical devices and process equipments. Ostrach [1], the initiator of the study of convection flow, made a technical note on the similarity solution of transient free convection flow past a semi infinite vertical plate by an integral method. Sakiadis [2] analyzed the boundary layer flow over a solid surface moving with a constant velocity. This boundary layer flow situation is quite different from the classical Blasius problem of boundary flow over a semi-infinite flat plate due to en- trainment of ambient fluid. Erickson et al. [3] extended the work of Sakiadis for suction or injection of a smooth surface.

The flow over a stretching surface is an important problem in many engineering processes with applications in industries such as extrusion, melt-spinning, the hot rolling, wire drawing, glass fiber production, manufacture of plastic and rubber sheets, cooling of a large metallic plate in a bath, which may be an electrolyte, etc. In industry, polymer sheets and filaments are manufactured by continuous extrusion of the polymer from a die to a windup roller, which is located at a finite distance away.

In many environmental and industrial flows the classical theory of Newtonian fluids is unable to explain the microfluid mechanical characteristics observed. Micropolar fluids are fluids with microstructure belonging to a class of complex fluids with nonsymmetrical stress tensor referred to as micromorphic fluids. Physically they represent many industrially important liquids consisting of randomly oriented particles suspended in a viscous medium. The classical theories of continuum mechanics are inadequate to explicate the microscopic manifestations of such complex hydrodynamic behaviour. Eringen [4] presented the earliest formulation of a general theory of fluid microcontinua taking into account the inertial characteristics of the substructure particles, which are allowed to sustain rotation and couple stresses. Later Eringen [5] generalized the theory to incorporate thermal effects in the so-called thermo micropolar fluid. The theory of micropolar fluids and its extension, the thermo micropolar fluid constitute suitable non-Newtonian hydrodynamic and thermo-hydrodynamic models which can simulate the flow dynamics of colloidal fluids, liquid crystals, polymeric suspensions, haemotological fluids etc. Many numerical studies of micropolar heat and mass transfer have been communicated in the literature. Hassanien and Gorla [6] investigated the heat transfer to a micropolar fluid from a non-isothermal stretching sheet with suction and blowing. Flow over a porous stretching sheet with strong suction or injection was examined by Kelson and Farell [7].

Transport of momentum and thermal energy in fluid saturated porous media with low porosities, such as rocks, soil, sand, etc., is commonly described by using Darcy's model for conservation of momentum and by using an energy equation based on the velocity field found from this model
[8]. In contrast to rocks, soil, sand and other media that do fall in this category, certain porous materials, such as foam metals and fibrous media, usually have high porosity. Raptis [9] studied the boundary layer flow of a micropolar fluid through a non-Darcian porous medium.

Magnetoconvection plays an important role in agriculture, petroleum industries, geophysics and in astrophysics. Important applications are found in the study of geological formations, in exploration and thermal recovery of oil and in the assessment of aquifers, geothermal reservoirs and underground nuclear waste storage sites. MHD flow has applications in metrology, solar physics and in motion of the earth's core. Also, it has applications in the field of stellar and planetary magnetospheres, aeronautics, chemical engineering and electronics. The effects of a transversely applied

magnetic field on the flow of an electrically conducting fluid past an impulsively started infinite isothermal vertical plate were studied by Soundalgekar et al. [10]. MHD effects on impulsively started vertical infinite plate with variable temperature in the presence of a transverse magnetic field were studied by Soundalgekar et al. [11]. The dimensionless governing equations were solved using the Laplace transform technique.

Radiative heat and mass transfer play an important role in manufacturing industries for the design of fins, steel rolling, nuclear power plants, and gas turbines. Various propulsion devices for aircraft, missiles, satellites and space vehicles are examples of such engineering applications. If the temperature of the surrounding fluid is rather high, radiation effects play an important role and this situation exists in space technology. In such cases, one has to take into account the effect of thermal radiation and mass diffusion. England and Emery [12] studied thermal radiation effects of an optically thin gray gas bounded by a stationary vertical plate. Radiation effects on mixed convection along an isothermal vertical plate were studied by Hossain and Takhar [13]. Raptis and Perdikis [14] studied the effects of thermal radiation and free convection flow past a moving vertical plate, the governing equations were solved analytically. Das *et al*. [15] analyzed radiation effects on flow past an impulsively started infinite isothermal vertical plate. Hayat and Qusim [16] proposed the effects of thermal radiation on MHD flow of a micropolar fluid with mass transfer. The radiation effect on steady free convection flow near isothermal stretching sheet in the presence of a magnetic field is studied by Ahmed [17].

The study of heat and mass transfer with chemical reaction is of great practical importance in many branches of science and engineering. Das et al. [18]studied the effects of mass transfer flow past an impulsively started infinite vertical plate with constant heat flux and chemical reaction. Anjalidevi and Kandasamy [19] studied effects of chemical reaction, heat and mass transfer on laminar flow along a semi-infinite horizontal plate. Pal and Chatterjee [20] studied heat and mass transfer in MHD non-Darcian flow of a micropolar fluid over a stretching sheet embedded in a porous media with nonuniform heat source and thermal radiation. Chamkha et al. [21] studied the coupled heat and mass transfer by MHD natural convection of micropolar fluid about a truncated cone in the presence of radiation and chemical reaction. Intensive studies have been carried out to investigate effects of chemical reaction on different flow types [22 -25].

Vajravelu and Rollins [26] studied the heat transfer characteristics in an electrically conducting fluid over a stretching sheet with variable wall temperature and internal heat generation or absorption. Mostafa and Shimaa [27] studied the MHD flow and heat transfer of a micropolar fluid over a stretching surface with heat generation and slip velocity. Jat et al. [28] studied the MHD flow and heat transfer near the stagnation point of a micropolar fluid over a stretching surface with heat generation/absorption. Abo-Eldahb and El Aziz [29] found the heat transfer in a micropolar fluid past a stretching surface embedded in a non-Darcian porous medium with heat generation. Mohammed Ibrahim [30] proposed the radiation and mass transfer effects on MHD free convection flow of a micropolar fluid past a stretching surface placed in a non-Darcian porous medium in presence of heat generation.

In all the above papers viscous dissipation is neglected. But when the motion is under strong gravitational field, or flow field is of extreme size, the viscous dissipative heat cannot be neglected. Rahman [31] analyzed the steady laminar free-forced convective flow and heat transfer of micropolar fluids past a vertical radiate isothermal permeable surface in the presence of viscous dissipation and Ohmic heating. Abel et al. [32] studied the MHD flow, and heat transfer with effects of buoyancy, viscous and Joules dissipation over a nonlinear vertical stretching porous sheet with partial slip. Hsiao and Lee [33] analyzed the conjugate heat and mass transfer for MHD mixed convection with viscous dissipation and radiation effect for viscoelastic fluid past a stretching sheet. Gebhart [34] has shown that the viscous dissipation effect plays an important role in natural convection in various devices processes on large scales (or large planets). Also, he pointed out that when the temperature is small, or when the gravitational field is of high intensity, viscous dissipations is more predominant in vigorous natural convection processes. Govardhan et al. [35] studied the radiation effect on MHD steady free convection flow of a gas at a stretching surface with a uniform free stream with viscous dissipation. Salem [36] investigated the effects of viscous dissipation and chemical reaction on MHD micropolar fluid along a permeable stretching sheet in non-Darcian porous medium with variable viscosity. Mahmoud [37] found that the effects of viscous dissipation and heat generation on MHD flow of a micropolar fluid over a moving permeable surface embedded in a non-Darcian porous medium.

However the interaction of chemical reaction with thermal radiation of an electrically conducting micropolar fluid past a stretching surface has received little attention. Hence an attempt is made to investigate the thermal radiation effects on a steady free convection flow near an isothermal vertical stretching sheet in the presence of a magnetic field, a non-Darcian porous medium, viscous dissipation and heat generation. The governing equations are transformed by using similarity transformation and the resultant dimensionless equations are solved numerically using the Runge-Kutta fourth order method with the shooting technique. The effects of various governing parameters on the velocity, temperature, concentration, skin-friction coefficient, the Nusselt number, and Sherwood number are shown in the figures and tables and analyzed in detail.

Mathematical Formulation

Let us consider a steady, two-dimensional laminar, free convection boundary layer flow of an electrically conducting dissipative and heat generating micropolar fluid through a porous medium bounded by a vertical isothermal stretching sheet coinciding with the plane $y = 0$, where the flow confined to $y > 0$. Two equal and opposite forces are introduced along the x' - axis so that the sheet is linearly stretched keeping the origin fixed (See Figure A). A uniformly distributed transverse magnetic field of strength B_0 is imposed along the y' - axis. The magnetic Reynolds number of the flow is taken to be small enough so that the induced distortion of the applied magnetic field can be neglected. It is also assumed that microscopic inertia term involving J (where J is the square of the characteristic length of microstructure) can be neglected for steady two-dimensional boundary layer flow in a micropolar fluid without introducing any

appreciable error in the solution. Under the above assumptions and upon treating the fluid saturated porous medium as continuum, including the non-Darcian inertia effects, and assuming that the Boussinesq approximation is valid, the boundary layer form of the governing equations can be written as (Willson [38], Nield and Bejan [39]).

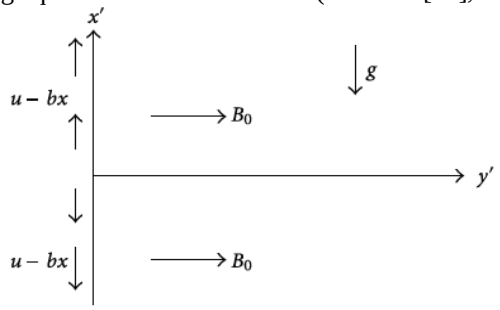

Figure A. Sketch of the physical model

Continuity equation

$$\frac{\partial u'}{\partial x'}+\frac{\partial v'}{\partial y'}=0 \qquad (1)$$

Momentum Equation

$$u'\frac{\partial u'}{\partial x'}+v'\frac{\partial u'}{\partial y'}=\nu\frac{\partial^2 u'}{\partial y'^2}+g\beta\left(T'-T'_\infty\right)+g\beta^*\left(C'-C'_\infty\right)+k_1\frac{\partial \sigma'}{\partial y'}-\frac{\sigma_0 B_0^2}{\rho}u'-\frac{\nu}{K}u'-C_1u'^2 \qquad (2)$$

Angular Momentum equation

$$G_1\frac{\partial^2\sigma}{\partial y'^2}-2\sigma-\frac{\partial u'}{\partial y'}=0 \qquad (3)$$

Energy equation

$$u'\frac{\partial T'}{\partial x'}+v'\frac{\partial T'}{\partial y'}=\frac{k_e}{\rho c_p}\frac{\partial^2 T'}{\partial y'^2}-\frac{1}{\rho c_p}\frac{\partial q_r}{\partial y'}+\frac{Q_0}{\rho c_p}\left(T'-T'_\infty\right)+\frac{\mu}{\rho c_p}\left(\frac{\partial u'}{\partial y'}\right)^2 \qquad (4)$$

Species equation

$$u'\frac{\partial C'}{\partial x'}+v'\frac{\partial C'}{\partial y'}=D\frac{\partial^2 C'}{\partial y'^2}-K'_r\left(C'-C'_\infty\right) \qquad (5)$$

Subject to the boundary conditions

$$u'=bx,\quad v'=0,\quad T'=T'_w,\quad C'=C'_w,\quad \sigma=0 \text{ at } y=0,$$

$$u'\to u'_\infty,\quad T'\to T'_\infty,\quad C'\to C'_\infty,\quad \sigma=0 \quad \text{as } y\to\infty \qquad (6)$$

where x' and y' are the coordinates along and normal to the sheet. u' and v' are the components of the velocity in the x' and y'- directions, respectively. σ, k_1 and G_1 are the microrotation component, coupling constant, and microrotation constant, respectively. k_e, C_1, K are the effective thermal conductivity, permeability of the porous medium, transport property related to the inertia effect. T' is fluid temperature, C' is fluid concentration. T'_w is the surface temperature, C'_w is the surface concentration, T'_∞ be the ambient temperature of fluid, C'_∞ is the ambient concentration of fluid, $\beta, \beta^*, u'_\infty$ and g are the coefficient of thermal expansion, coefficient of concentration expansion, free steam velocity, and acceleration due to gravity, respectively. σ_0 be the electrical conductivity, ρ be the fluid density, ν be the kinematic viscosity, μ be the dynamic viscosity, c_p be the specific heat at constant pressure of the

fluid, Q_0 be the volumetric rate of heat generation, *b* be the constant, *D* be the diffusion coefficient, and Kr' is the chemical reaction parameter.

By using the Rosseland approximation (Brewster [40]), the radiative heat flux in y' direction is given by

$$q_r = -\frac{4\sigma^*}{3k^*}\frac{\partial T'^4}{\partial y'} \tag{7}$$

where σ^* is the Stefan-Boltzmann constant and k^* is the mean absorption coefficient. By using equation (7), the energy equation (4) becomes

$$u'\frac{\partial T'}{\partial x'} + v'\frac{\partial T'}{\partial y'} = \frac{k_e}{\rho c_p}\frac{\partial^2 T'}{\partial y'^2} + \frac{4\sigma^*}{3k^*\rho c_p}\frac{\partial^2 T'^4}{\partial y'^2} + \frac{Q_0}{\rho c_p}\left(T' - T'_\infty\right) + \frac{\mu}{\rho c_p}\left(\frac{\partial u'}{\partial y'}\right)^2 \tag{8}$$

It is convenient to make the governing equations and conditions dimensionless by using

$$x = \frac{bx'}{u'_\infty}, \quad y = \frac{by'}{u'_\infty}R, \quad u = \frac{u'}{u'_\infty}, \quad v = \frac{v'}{u'_\infty}R, \quad R = \frac{u'_\infty}{\sqrt{c\nu}}, \quad \theta = \frac{T' - T'_\infty}{T'_w - T'_\infty}, \quad \phi = \frac{C' - C'_\infty}{C'_w - C'_\infty}$$

$$M = \frac{\sigma_0 B_0^2}{\rho b}, \qquad Gr = \frac{g\beta\left(T'_w - T'_\infty\right)}{bu'_\infty}, \qquad Gc = \frac{g\beta^*\left(C'_w - C'_\infty\right)}{bu'_\infty}, \qquad Da^{-1} = \frac{\nu}{Kb} \qquad \gamma = \frac{C_1 u'_\infty}{b}$$

$$\Pr = \frac{\mu c_p}{k} \qquad F = \frac{kk^*}{4\sigma^* T_\infty^3}, \quad r = \frac{T'_w - T'_\infty}{T'_\infty} \quad , \qquad Ec = \frac{u_\infty^2}{c_p(T_w - T_\infty)} \; Q = \frac{Q_0}{b\rho c_p} \tag{9}$$

$$Sc = \frac{\nu}{D} \qquad Kr = \frac{Kr'}{b}$$

where *R* is the Reynolds number.

In view of the equation (8), the equations (1), (2), (3), (8) and (5) reduce to the following non-dimensional form.

$$\frac{\partial u}{\partial x} + \frac{\partial v}{\partial y} = 0 \tag{10}$$

$$u\frac{\partial u}{\partial x} + v\frac{\partial u}{\partial y} = \frac{\partial^2 u}{\partial y^2} + Gr\theta + Gc\phi + N\frac{\partial \sigma}{\partial y} - \left(M + \frac{1}{Da}\right)u - \gamma u^2 \tag{11}$$

$$G\frac{\partial^2 \sigma}{\partial y^2} - 2\sigma - \frac{\partial u}{\partial y} = 0 \tag{12}$$

$$u\frac{\partial \theta}{\partial x} + v\frac{\partial \theta}{\partial y} = \frac{1}{\Pr}\frac{\partial^2 \theta}{\partial y^2} + \frac{4}{3F\Pr}\left[\left(1 + r\theta\right)^3\frac{\partial^2 \theta}{\partial y^2} + 3r\left(1 + r\theta\right)^2\left(\frac{\partial \theta}{\partial y}\right)^2\right] + Q\theta + Ec\left(\frac{\partial u}{\partial y}\right)^2 \tag{13}$$

$$u\frac{\partial \phi}{\partial x} + v\frac{\partial \phi}{\partial y} = \frac{1}{Sc}\frac{\partial^2 \phi}{\partial y^2} - Kr\phi \tag{14}$$

The corresponding boundary conditions are

u = x, v = 0, $\sigma = 0$, $\theta = 1$, $\phi = 1$ *at y = 0,*

u = 1, $\sigma = 0$, $\theta = 0$, $\phi = 0$ *as* $y \to \infty$ (15)

Proceeding with the analysis, we define a stream function $\psi(x, y)$ such that

$$u = \frac{\partial \psi}{\partial y}, \quad v = -\frac{\partial \psi}{\partial x} \tag{16}$$

Now, let us consider the steam function as if

$$\psi(x, y) = f(y) + xg(y) \tag{17}$$

$$\sigma = xh(y) \tag{18}$$

In view of equation (16) – (18), the continuity equation (10) is identically satisfied and the momentum equation (11), angular momentum equation (12), energy equation (13) and species equation (14) becomes

$$\frac{\partial \psi}{\partial y}\frac{\partial^2 \psi}{\partial x \partial y} - \frac{\partial \psi}{\partial x}\frac{\partial^2 \psi}{\partial y^2} = \frac{\partial^3 \psi}{\partial y^3} + Gr\theta + Gc\phi - \left(M + \frac{1}{Da}\right)\frac{\partial \psi}{\partial y} + \gamma\left(\frac{\partial \psi}{\partial y}\right)^2 \tag{19}$$

$$G\frac{\partial^2 \sigma}{\partial y^2} - 2\sigma - \frac{\partial u}{\partial y} = 0 \tag{20}$$

$$\frac{\partial \psi}{\partial y}\frac{\partial \theta}{\partial x} - \frac{\partial \psi}{\partial x}\frac{\partial \theta}{\partial y} = \frac{1}{\Pr}\frac{\partial^2 \theta}{\partial y^2} + \frac{4}{3F\Pr}\left[(1+r\theta)^3\frac{\partial^2 \theta}{\partial y^2} + 3r(1+r\theta)^2\left(\frac{\partial \theta}{\partial y}\right)^2\right] + Q\theta + Ec\left(\frac{\partial^2 \psi}{\partial y^2}\right)^2 \tag{21}$$

$$\frac{\partial \psi}{\partial y}\frac{\partial \phi}{\partial x} - \frac{\partial \psi}{\partial x}\frac{\partial \phi}{\partial y} = \frac{1}{Sc}\frac{\partial^2 \phi}{\partial y^2} - Kr\phi \tag{22}$$

and the boundary conditions (15) become

$$\frac{\partial \psi}{\partial y} = x, \quad \frac{\partial \psi}{\partial x} = 0, \quad h = 0, \ \theta = 1, \ \phi = 1 \quad \text{at } y = 0$$

$$\frac{\partial \psi}{\partial y} \to 1, \quad h \to 0, \ \theta \to 0, \ \phi \to 0 \quad \text{as} \quad y \to \infty \tag{23}$$

In equations (19), (20), (21), (22) and equating coefficient of x^0 and x^1, we obtain the coupled non-linear ordinary differential equations

$$f''' + f''g - f'g' - \left(M + \frac{1}{Da}\right)f' - \gamma f'^2 + Gr\theta + Gc\phi = 0 \tag{24}$$

$$g''' + gg'' - (g')^2 - \left(M + \frac{1}{Da}\right)g' - 2\gamma f'g' + Nh' = 0 \tag{25}$$

$$Gh'' - 2h - g'' = 0 \tag{26}$$

$$\left(3F + 4(1+r\theta)^3\right)\theta'' + 3\Pr Fg\theta' + 12r(1+r\theta)^2\theta'^2 + 3F\Pr Q\theta + 3F\Pr Ecf''^2 = 0 \tag{27}$$

$$\phi'' + Scg\phi' - KrSc\phi = 0 \tag{28}$$

where a prime denotes differentiation with respect to *y*.

In view of equations (17), (18) , the boundary condition (23) reduce to

$$f = 0, \quad f' = 0, \quad g = 0, \quad g' = 1, \quad h = 1, \quad \theta = 1, \quad \phi = 1 \quad \text{at} \quad y = 0$$

$$f' \to 1, \quad g' \to 0, \quad h \to 0, \quad \theta \to 0, \quad \phi \to 0 \quad \text{as} \quad y \to \infty \tag{29}$$

The physical quantities which are of importance for this problem are the skin-friction coefficient, Nusselt number and Sherwood number, which are defined by

The shear stress at the stretching surface is given by

$$\tau_w = (\mu + k)\left(\frac{\partial u'}{\partial y'}\right)_{y'=0} + k(\sigma)_{y'=0} = \rho\nu bR\left(\frac{\partial u}{\partial y}\right)_{y=0}$$

$$= \rho\nu bR\left(f''(0) + xg''(0)\right) \quad (30)$$

The skin-friction coefficient $C_f = \dfrac{\tau_w}{\frac{1}{2}\rho u_\infty^2} = \dfrac{2}{R}\left(f''(0) + xg''(0)\right)$ (31)

The wall heat flux is given by

$$q_w = -k\left(\frac{\partial T'}{\partial y'}\right)_{y'=0} = -k\frac{bR}{u_\infty}\left(\frac{\partial T}{\partial y}\right)_{y=0} = -k\frac{bR}{u_\infty}\left(T_w' - T_\infty'\right)\theta'(0)$$

Nusselt number $Nu = \dfrac{q_w}{k\left(T_w' - T_\infty'\right)} = \dfrac{bR}{u_\infty}\theta'(0)$ (32)

The wall mass flux is given by

$$m_w = -D\left(\frac{\partial C'}{\partial y'}\right)_{y'=0} = -D\frac{bR}{u_\infty}\left(\frac{\partial C}{\partial y}\right)_{y=0} = -D\frac{bR}{u_\infty}\left(C_w' - C_\infty'\right)\phi'(0)$$

Sherwood number $Sh = \dfrac{m_w}{D\left(C_w' - C_\infty'\right)} = \dfrac{bR}{u_\infty}\phi'(0)$ (33)

Solution of the Problem

The shooting method for linear equations is based on replacing the boundary value problem by two initial value problems and the solutions of the boundary value problem is a linear combination between the solutions of the two initial value problems. The shooting method for the nonlinear boundary value problem is similar to the linear case, except that the solution of the nonlinear problem cannot be simply expressed as a linear combination of the solutions of the two initial value problems. Instead, we need to use a sequence of suitable initial values for the derivatives such that the tolerance at the end point of the range is very small. This sequence of initial values is given by the secand method, and we use the fourth order Runge-Kutta method to solve the initial value problems.

The full equations (24) – (28) with the boundary conditions (29) were solved numerically using the Runge-Kutta method algorithm with a systematic guessing $f''(0), g''(0), h'(0), \theta'(0)$ and $\phi'(0)$ by the shooting technique until the boundary conditions at infinity $f'(y)$ decay exponentially to one, also $g'(0), h(y), \theta(y)$ and $\phi(y)$ to zero. The functions $f', g', -h, \theta$ and ϕ are shown in figures.

Results and Discussion

As a result of the numerical calculations, the dimensionless velocity, angular velocity, temperature, and concentration distributions for the flow under consideration are obtained and their behavior has been discussed for variations in the governing parameters, namely, the thermal Grashof number *Gr*, solutal Grashof number *Gc*, magnetic field parameter *M*, Darcy number *Da*, , porous medium inertia coefficient γ , vortes viscosity parameter *N*, microrotation parameter *G*, Prandtl number *Pr*, radiation parameter *F*, the parameter of relative difference between the temperature of the sheet and temperature far *r*, heat generation parameter *Q*, Eckert number *Ec*, Schmidt number *Sc*, and chemical reaction parameter *Kr*. In the present study, the following default parametric values are adopted: *Gr = 1.0, Gc =1.0, M = 0.01, Da = 100,* γ *= 0.1, N = 0.1, G = 2.0, Pr = 0.71, F = 1.0, r = 0.05, Q = 0.1, Ec = 0.05, Sc = 0.6, Kr = 0.5*. All graphs therefore correspond to these unless specifically indicated on the appropriate graph.

In order to assess the accuracy of our computed results, the present results have been compared with Abo-Eldahab and ELaziz [30] for different values of *G* as shown in Figure 1 with Gc = 0.0, *F* = 0.0, *r = 0.0, Ec = 0.0, Sc = 0.0 and Kr = 0.0*. It is observed that the agreements with the solution of angular velocity profiles are excellent.

Figure 2(a) shows the variation of the dimensionless velocity component f' for several sets of values of thermal Grashof number *Gr*. As expected, it is observed that there is a rise in the velocity due to enhancement of thermal buoyancy force. The variation of the dimensionless velocity component f' for several sets of values of solutal Grashof number Gc is depicted in Figure 2(b). As expected, the fluid velocity increases and the peak value is more distinctive due to the increase in the species buoyancy force. It should be mentioned herein that the profiles of g', h, θ and ϕ were found to be insensible to change in *Gr* and *Gc*, therefore, not shown herein for brevity.

The effect of variation of the magnetic parameter *M* on the velocity (f' and g'), angular velocity $-h$, temperature θ, and concentration ϕ profiles is presented in Figures 3(a)– 3(e) respectively. It is well known that the application of a uniform magnetic field normal to the flow direction gives rise to a force called Lorentz. This force has the tendency to slow down the velocity of the fluid and angular velocity of microrotation in the boundary layer and to increase its temperature and concentration. This is obvious from the decreases in the velocity profiles, angular velocity of microrotation profiles, while temperature and concentration profiles increases, presented in Figures. 3(a) – 3(e).

Figures 4(a)–4(e) present typical profiles for the variables of the fluid's x-component of velocity (f' and g'), angular velocity $-h$, temperature θ, and concentration ϕ for different values of Darcy number *Da*. It is noted that values of *Da* increase the fluid velocities and angular velocity increases, while temperature and concentration of the fluid decrease.

Figures 5(a)–5(e) present the typical profiles for the variables of the fluid's x-component of velocity (f' and g'), angular velocity $-h$, temperature θ and concentration ϕ for different values of the porous medium inertia coefficient γ. Obviously, the porous medium inertia effects constitute resistance to the flow. Thus as the inertia coefficient increases, the resistance to the flow increases, causing the fluid flow in the porous medium to slow down and the temperature and concentration increase and, therefore, as γ increases f', g', and $-h$ decreases while the temperature θ and concentration ϕ increase.

Figures 6(a)–6(e) present the typical profiles for the variables of the fluid's x-component of velocity (f' and g'), angular velocity $-h$, temperature θ, and concentration ϕ for different values of the vortex viscosity parameter N. Increases in the values of *N* have a tendency to increase f', $-h$, θ, and ϕ and to decrease g'.

Figure 7 is a plot of the dimensionless angular velocity $-h$ profiles for different values of the presence of the microrotation parameter *G*. The curves illustrate that, as the values of *G* increases, the angular velocity $-h$, as expected, decreases with an increase in the boundary layer thickness as the maximum moves away from the sheet. Of course, when the viscosity of the fluid decreases the angular velocity of additive increases.

Figure 8(a) Illustrates the dimensionless velocity component f' for different values of the Prandtl number *Pr*. The numerical results show that the effect of increasing values of the Prandtl number results in a decreasing velocity. From Figure 8(b), it is observed that an increase in the Prandtl number results in a decrease of the thermal boundary layer thickness and in general lower average temperature within the boundary layer. The reason is that smaller values of *Pr* are equivalent to increasing the thermal conductivities, and therefore heat is able to diffuse away from the heated plate more rapidly than for higher values of *Pr*. Hence in the case of smaller Prandtl numbers as the boundary layer is thicker, the rate of heat transfer is reduced.

The effect of the radiation parameter *F* on the dimensionless velocity component f' and dimensionless temperature is shown in Figures 9 (a) and 9 (b) respectively. Figure 9 (a) shows that velocity component f' decreases with an increase in the radiation parameter *F*. From Figure 9(b) it is seen that the temperature decreases as the radiation parameter *F* increases. This result qualitatively agrees with expectations, since the effect of radiation is to decrease the rate of energy transport to the fluid, thereby decreasing the temperature of the fluid.

The influence of the parameter of relative difference between the temperature of the sheet and the temperature far away from the sheet r on dimensionless velocity f' and temperature profiles are plotted in Figures 10(a) and 10(b), respectively. Figure 10(a) shows that dimensionless velocity f' increases with an increase in r. It is observed that the temperature increases with an increase in *r* (Figure 10(b)).

Figures 11(a) and 11(b) illustrate the respective changes in the profiles of f' and θ as the heat generation coefficient Q is changed. It is clear from Figures 11(a) and 11(b) that increasing in the values of Q produces increases in the velocity f' and temperature θ distributions of the fluid. This is expected since heat generation $(Q > 0)$ causes the thermal boundary layer to become thicker and the fluid to be warmer. This enhances the effects of thermal buoyancy of the driving body force due to mass density variations which are coupled to the temperature distribution and therefore increasing the fluid velocity distribution. No figures for g', $-h$ and ϕ are presented for the same reason as mentioned before.

Figures 12 (a) and 12(b) display the respective changes in the profiles of f' and θ as the Eckert number *Ec* is changed. The positive Eckert number implies cooling of the plate i.e., loss of heat from the plate to the fluid. Hence, greater viscous dissipative heat causes a rise in the temperature as well as the velocity, which is evident from Figures 12(a) and 12(b).

The influence of the Schmidt number *Sc* on the dimensionless velocity f' and concentration profiles is plotted in Figures 13(a) and 13(b), respectively. As the Schmidt number increases the concentration decreases. This causes the concentration buoyancy effects to decrease yielding a reduction in the fluid velocity. The reductions in the velocity and concentration profiles are accompanied by simultaneous reductions in the velocity and concentration boundary layers. These behaviors are clear from Figures 13(a) and 13(b).

The effects of the chemical reaction parameter *Kr* on dimensionless velocity component f' and concentration profiles are plotted in figures 14(a) and 14(b). As the chemical reaction parameter increases the velocity and concentration profiles are decreases. These behaviors are clear from Figures 14(a) and 14(b).

Finally, in order to verify the proper treatment of the present problem, we will compare the obtained numerical solution with results reported by Abo-Eldahab and El Aziz [30]. Table 1 presents comparisons for the velocities of $f''(0)$ and $g''(0)$ values for various *M* values. These comparisons show excellent agreement between the results.

Table 2 illustrates the missing wall functions for velocity, angular velocity, temperature, and concentration functions. These quantities are useful in the evaluation of wall shear stresses, gradient of angular velocity, surface heat transfer rate, and mass transfer rate. The results are obtained for r = 0.05 and different values of the thermal Grashof number Gr, solutal Grashof number Gc, magnetic field parameter *M*, Darcy number *Da*, porous medium inertia coefficient γ, vortes viscosity parameter *N*, microrotation parameter *G*, radiation parameter *F*, the parameter of relative difference between the temperature of the sheet and temperature far away from the sheet r, Prandtl number Pr, heat generation parameter *Q*, Eckert number *Ec*, and Schmidt number Sc. Table 1 indicates that increasing the values of the Grashof number *Gr* and solutal Grashof number *Gc* results in an increase in the values of $f''(0)$. This is because as *Gr* and *Gc* increase, the momentum boundary layer thickness decreases and, therefore, an increase in the values of $f''(0)$ occurs. The results indicate that a distinct fall in the skin-friction coefficient in the *x*-direction ($f''(0)$ and $g''(0)$), the surface heat transfer rate $-\theta'(0)$, and mass transfer rate $-\phi'(0)$, while gradient of angular velocity $h'(0)$ increases accompanies a rise in the magnetic field parameter *M*. Increases in the values of *Da* have the effect of increasing the skin-friction function $f''(0)$, heat transfer rate $-\theta'(0)$ and mass transfer rate $-\phi'(0)$ while the gradient of angular velocity $h'(0)$ and the skin-friction function $g''(0)$ slightly decreases as *Da* increases. Further, the influence of the porous medium inertia coefficient γ on the wall shear stresses, gradient of angular velocity, surface heat transfer, and surface mass transfer rate is the same as that of the inverse Darcy number *Da*, since it also represents resistance to the flow. Namely, as γ increases, $f''(0)$, $\theta'(0)$, $\phi'(0)$ decrease while $g''(0)$, $h'(0)$ slightly increases, respectively.

From Table 3 for given values of *Gr, Gc, M, Da,* γ, *Sc* and *Kr* an increase in the values of microrotation parameter *N* leads to reduction in the skin-friction function $g''(0)$, $\theta'(0)$ and $\phi'(0)$ while the skin-friction function $f''(0)$ and gradient of angular velocity $h'(0)$, increase as *N* increases. The skin friction $f''(0)$ increases and the gradient of angular velocity $h'(0)$ is decreased as the microrotation parameter *G* increases, while the skin-friction coefficient in the *x*-directions $g''(0)$ heat transfer rate $-\theta'(0)$, and mass transfer rate $-\phi'(0)$ are insensible to change in *G*. Increasing the values of heat generation parameter *Q* or Eckert number Ec results in an increase in the values of $f''(0)$ and the heat transfer rate $-\theta'(0)$ decreases. It is observed that the magnitude of the wall temperature gradient increases as Prandtl number *Pr* or radiation parameter *F* increases.

From Table 4, the magnitude of the wall concentration increases with an increase in the Schmidt number *Sc* or chemical reaction parameter *Kr* . Furthermore, the negative values of the wall temperature and concentration gradients, for all values of the dimensionless parameters, are indicative of the physical fact that the heat flows from the sheet surface to the ambient fluid.

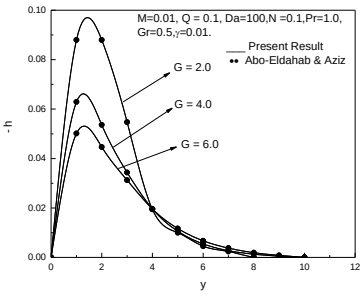

Fig.1: Comparison of angular velocity Profiles.

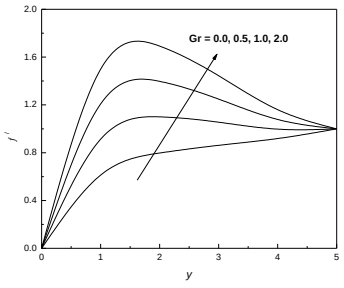

Fig 2(a) Variation of the velocity component f' with *Gr*

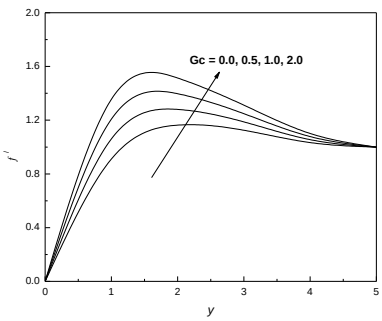

Fig 2(b) Variation of the velocity component f' with *Gc.*

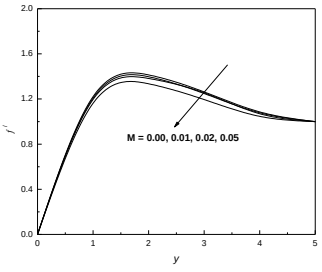

Fig .3(a) Variation of the velocity component f' with *M*.

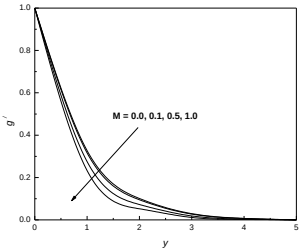

Fig. 3(b) Variation of the velocity component g' with *M*

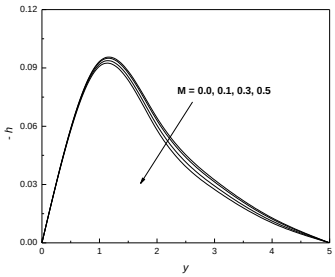

Fig 3(c) Variation of the velocity component $-h$ with *M*

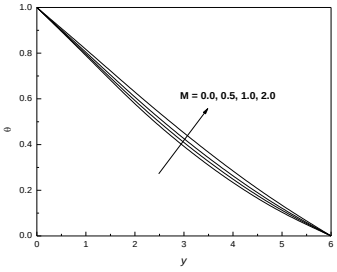

Fig 3(d) Variation of the velocity component θ with M.

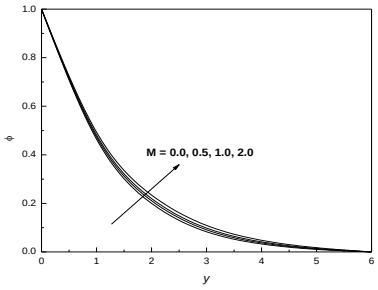

Fig 3(e) Variation of the velocity component ϕ with M.

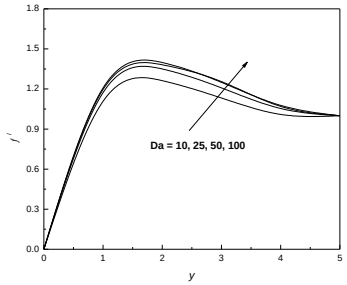

Fig. 4(a) Variation of the velocity component f' with Da

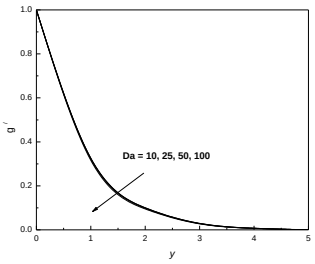

Fig. 4(b) Variation of the velocity component g' with Da.

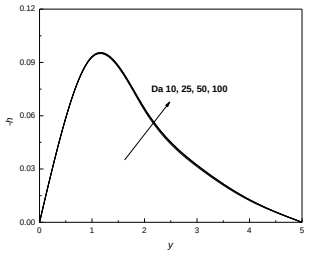

Fig 4(c) Variation of the velocity component $-h$ with Da.

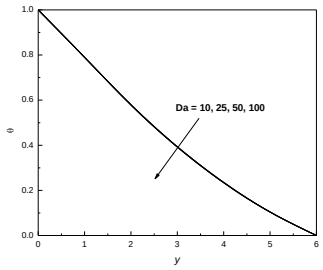

Fig. 4(d) Variation of the velocity component θ with Da

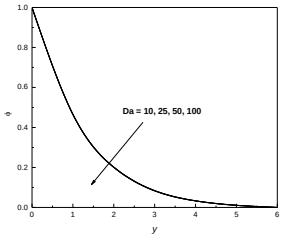

Fig 4(e) Variation of the velocity component ϕ with Da.

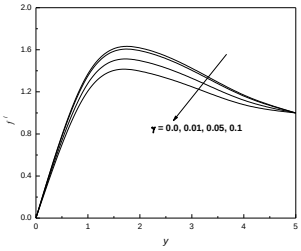

Fig. 5(a) Variation of the velocity component f' with γ.

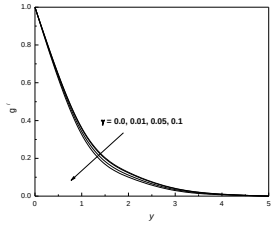

Fig 5(b) Variation of the velocity component g' with γ.

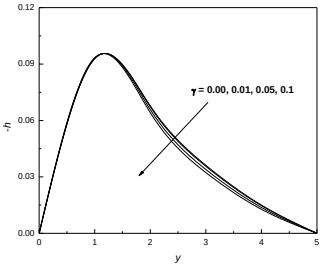

Fig. 5(c) Variation of the velocity component - h with γ.

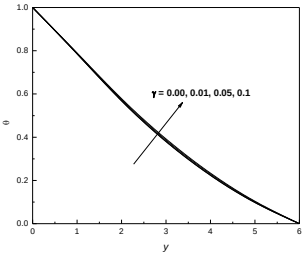

Fig 5(d) Variation of the velocity component θ with γ.

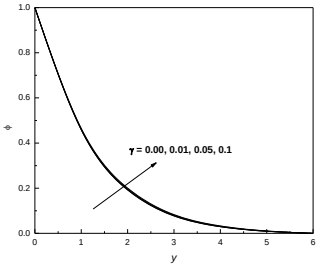

Fig 5(e) Variation of the velocity component ϕ with γ.

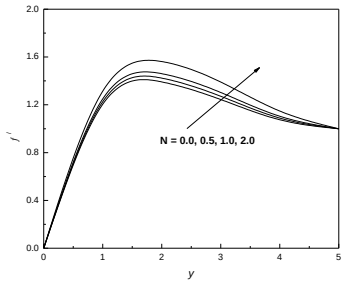

Fig 6(a) Variation of the velocity component f' with N

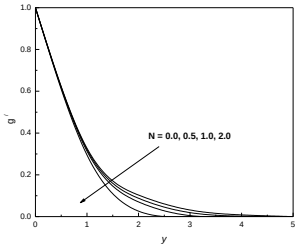

Fig 6(b) Variation of the velocity component g' with N

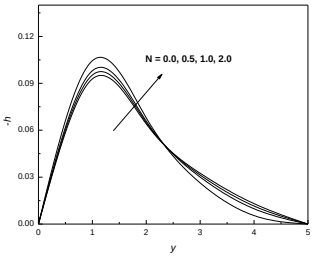

Fig 6(c) Variation of the velocity component - h with N.

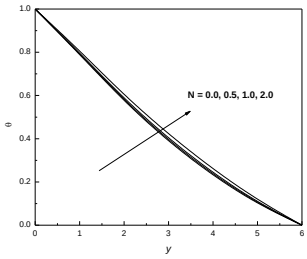

Fig 6(d) Variation of the velocity component θ with N

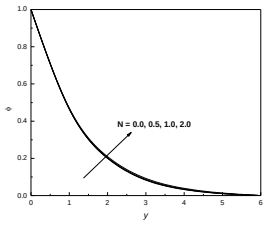

Fig 6(e) Variation of the velocity component ϕ with N.

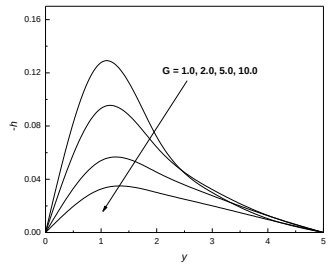

Fig. 7 Variation of the velocity component - h with G.

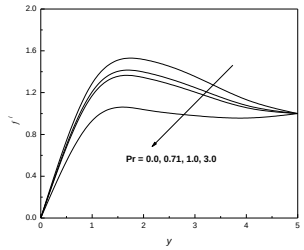

Fig 8(a) Variation of the velocity component f' with Pr.

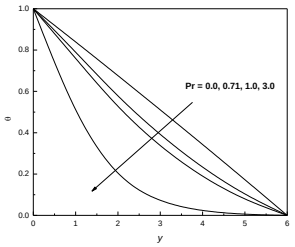

Fig 8(b) Variation of the velocity component θ with Pr.

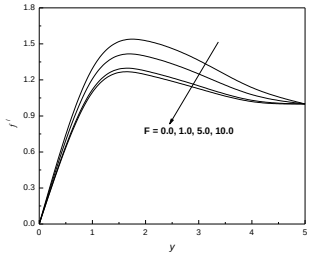

Fig 9(a) Variation of the velocity component f' with F.

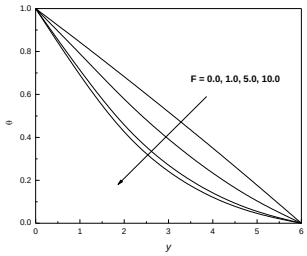

Fig 9(b) Variation of the velocity component θ with F.

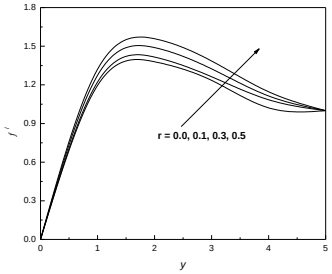

Fig 10(a) Variation of the velocity component f' with r.

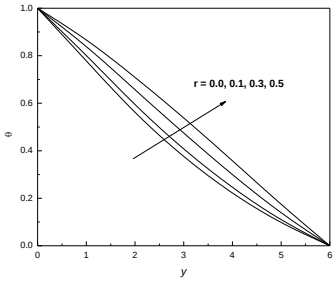

Fig 10(b) Variation of the velocity component θ with r.

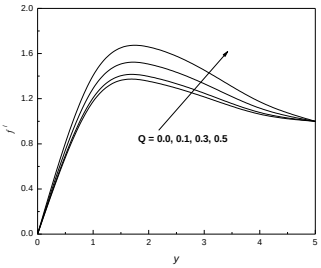

Fig 11(a) Variation of the velocity component f' with Q.

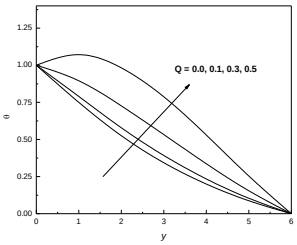

Fig 11(b) Variation of the velocity component θ with Q.

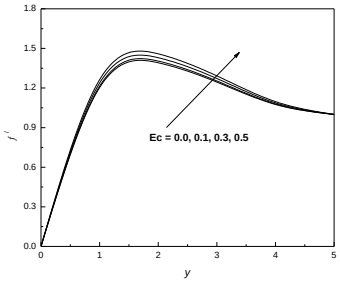

Fig 12(a) Variation of the velocity component f' with Ec

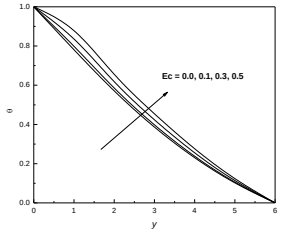

Fig 12(b) Variation of the velocity component θ with Ec.

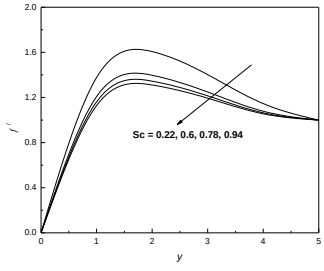

Fig 13(a) Variation of the velocity component f' with Sc.

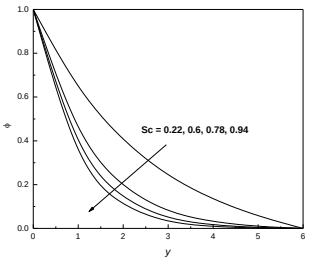

Fig 13(b) Variation of the velocity component ϕ with Sc.

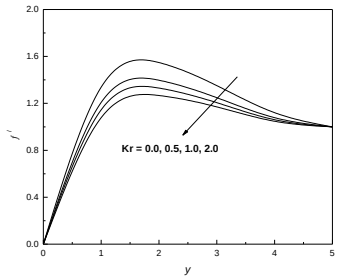

Fig 14(a) Variation of the velocity component f' with *Kr*

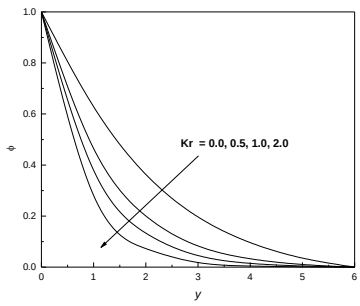

Fig 14(b) Variation of the velocity component ϕ with *Kr*

Table 1 Comparison of the present results with the literature results given by Abo-Eldahab E M and Aziz M A El [23], *Gc = 0.0, F = 0.0, r = 0.0, Sc = 0.0. Pr =1.0, Da = 100, γ = 0.01, N1 = 0.1, G = 2, Gr = 0.5, Q = 0.1.*

M	$f''(0)$		$g''(0)$	
	Present	Abo-Eldahab [30]	Present	Abo-Eldahab[30]
0.1	0.67059875	0.6708520	-1.0002147	-0.998951
0.2	0.57169871	0.5717493	-1.0002075	-0.998905

Table 2 Variation of $f'', g'', -h', \theta'$ and ϕ' at the plate with *Gr, Gc, M, Da and* γ *for N = 0.1, G = 2.0, Pr = 0.71, F = 1.0, r = 0.05, Q = 0.1, Ec = 0.05, Sc = 0.6, Kr = 0.5.*

Gr	*Gc*	*M*	*Da*	γ	$f''(0)$	$g''(0)$	$h'(0)$	$-\theta'(0)$	$-\phi'(0)$
1.0	1.0	0.01	100	0.1	2.03879	-1.0669	0.263381	0.221525	0.698487
2.0	1.0	0.01	100	0.1	3.05663	-1.09305	0.267723	0.190593	0.69596
3.0	1.0	0.01	100	0.1	4.06781	-1.11759	0.271691	0.148666	0.693639
1.0	2.0	0.01	100	0.1	2.7094	-1.08133	0.26557	0.206615	0.697201
1.0	3.0	0.01	100	0.1	3.37401	-1.09525	0.267659	0.18842	0.695971
1.0	1.0	0.03	100	0.1	2.01038	-1.07481	0.26414	0.221955	0.698037
1.0	1.0	0.05	100	0.1	1.98296	-1.08271	0.264898	0.222336	0.697586
1.0	1.0	0.01	10	0.1	1.91849	-1.10242	0.266785	0.223097	0.696464
1.0	1.0	0.01	50	0.1	2.02446	-1.07086	0.26376	0.221746	0.698262
1.0	1.0	0.01	100	0.3	1.82487	-1.14747	0.276459	0.220016	0.690858
1.0	1.0	0.01	100	0.5	1.69724	-1.20516	0.28477	0.218282	0.68592

Table 3 Variation of $f'', g'', -h', \theta'$ and ϕ' at the plate with *G, Pr, N, F, Q, Ec for Gr = 1.0, Gc =1.0, M = 0.01, Da = 100, Sc = 0.6, Kr = 0.5.*

G	*Pr*	*N*	*F*	*Q*	*Ec*	$f''(0)$	$g''(0)$	$h'(0)$	$-\theta'(0)$	$-\phi'(0)$
2	0.71	0.1	1.0	0.1	0.05	2.03879	-1.0669	0.263381	0.221525	0.698487
3	0.71	0.1	1.0	0.1	0.05	2.03789	-1.06794	0.192267	0.221645	0.698542
4	0.71	0.1	1.0	0.1	0.05	2.03734	-1.06859	0.152723	0.221716	0.698571
2	1.0	0.1	1.0	0.1	0.05	1.9971	-1.0653	0.263064	0.242647	0.698668
2	2.0	0.1	1.0	0.1	0.05	1.84742	-1.05963	0.261965	0.345313	0.699296
2	0.71	0.3	1.0	0.1	0.05	2.04717	-1.0567	0.264163	0.220518	0.698164
2	0.71	0.5	1.0	0.1	0.05	2.05609	-1.04641	0.264993	0.219448	0.697816
2	0.71	0.1	2.0	0.1	0.05	1.99298	-1.06515	0.263036	0.246632	0.698684
2	0.71	0.1	3.0	0.1	0.05	1.9671	-1.06416	0.262843	0.262791	0.698794
2	0.71	0.1	1.0	0.2	0.05	2.08389	-1.06854	0.263693	0.171505	0.698309
2	0.71	0.1	1.0	0.3	0.05	2.13599	-1.07043	0.264052	0.115424	0.698102
2	0.71	0.1	1.0	0.1	0.07	2.04179	-1.067	0.263398	0.212343	0.698477
2	0.71	0.1	1.0	0.1	0.1	2.04634	-1.06715	0.263424	0.198443	0.698462

Table 4 Variation of $f'', g'', -h', \theta'$ and ϕ' at the plate with *Sc and Kr for Gr = 1.0, Gc =1.0, M = 0.01, Da = 100, G = 2.0, Pr = 0.71, N = 0.1, F = 1.0, Q = 0.1, Ec = 0.05.*

Sc	*Kr*	$f''(0)$	$g''(0)$	$h'(0)$	$-\theta'(0)$	$-\phi'(0)$
0.6	0.5	1.87502	-1.06177	0.262497	0.213985	1.19009
0.78	0.5	1.97791	-1.06484	0.263009	0.223483	0.806176
0.94	0.5	1.93518	-1.06343	0.262759	0.22477	0.893162
0.6	1.0	1.95391	-1.06412	0.262888	0.224133	0.894788
0.6	2.0	1.85936	-1.06118	0.262382	0.226705	1.19012

References

[1] S. Ostrach, "An Analysis of Laminar Free-Convection Flow and Heat Transfer about a Flat Plate Parallel to the Direction of the Generating Body Force," Technical Note, NACA Report, Washington, 1952.

[2] B. C. Sakiadis, "Boundary-Layer Behavior on Continuous Solid Surfaces: I. Boundary-Layer Equations for Two- Dimensional and Axisymmetric Flow," *AIChE Journal*, Vol. 7, No. 1, 1961, pp. 26-28.

[3] L. E. Erickson, L. T. Fan and V. G. Fox, "Heat and Mass Transfer on a Moving Continuous Flat Plate with Suction or Injection," *Industrial Engineering and Chemical Fundamentals*, Vol. 5, No. 1, 1966, pp. 19-25.

[4] A.C. Eringen, Theory of micropolar fluids, *J. Math. and Mech.*, **16**, pp. 1–18, 1966.

[5] A.C. Eringen, Theory of thermomicrofluids, *J. Mathematical Analysis and Applications*, **38**, pp. 480–496, 1972.

[6] I.A. Hassanien, R. S.R. Gorla, Mixed convection boundary layer flow of a micropolar fluid near a stagnation point on a horizontal cylinder, *Acta Mech.*, **84**, pp. 191–199, 1990.

[7] N.A. Kelson, T.W. Farrell, Micropolar flow over a porous stretching sheet with strong suction or injection, *Int. Comm. Heat Mass Transfer*, **28**, pp. 479–488, 2001.

[8] M Kaviany (1991), Principles of heat transfer in porous media, 2nd edition, Springer-verlag, New-York.

[ ] Raptis A. (2000): Boundary layer flow of a micropolar fluid through a porous medium. Journal of Porous Media 3(1), 95-97

[10] V.M Soundalgekar ., S.K Gupta and R.N Aranake (1979): Free convection currents on MHD Stokes problem for a vertical plate. – Nuclear Engg. Des, vol.51, pp.403-407.

[11] V.M Soundalgekar ., S.K Gupta and N.S Birajdar (1979): Effects of mass transfer and free convection currents on MHD Stokes problem for a vertical plat. – Nuclear Engg. Des, vol.53, pp.339-346.

[12] W.G England and A.F Emery (1969): *Thermal radiation effects on the laminar free convection boundary layer of an absorbing gas.* – Journal of Heat Transfer, vol.91, pp.37-44.

[13] M.A Hossain and H.S Takhar (1996): *Radiation effect on mixed convection along a vertical plate with uniform surface temperature.* – Heat and Mass Transfer, vol.31, pp.243-248.

[14] A. Raptis and C. Perdikis (1999): *Radiation and free convection flow past a moving plate.* – International Journal of Applied Mechanics and Enginnering, vol.4, pp.817-821.

[15] U.N Das., R.K Deka and V.M Soundalgekar (1996): *Radiation effects on flow past an impulsively started vertical infinite plate.* – Journal of Theoretical Mechanics, vol., pp.111.

[16] T Hayat and M Qusim (2010), Effects of thermal radiation on unsteady magnetohydrodynamic flow of a micropolar fluid with heat and mass transfer, Z. Naturforsch, 65 a, pp. 950-960.

[17] Ahmed, Y., Ghaly, and M.E El sayed, Elbarbary (2002), Radiation effect on MHD free Convection flow of a gas at a stretching surface with a uniform free stream, Journal of Applied Mathematics, Vol. 2, pp. 93-103.

[18] U.N Das., R. Deka, and V.M Soundalgekar, (1994). Effects of mass transfer on flow past an impulsively started infinite vertical plate with constant heat flux and chemical reaction. *J. Forshung Im Ingenieurwesen-Engineering Research Bd*, 60, 284-287.

[19] S.P Anjalidevi, and R Kandasamy, (1999). Effects of chemical reaction, heat and mass transfer on laminar flow along a semi infinite horizontal plate. Heat and Mass Transfer, 35, 465-467.

[20] D. Pal and S. Chatterjee, "Heat and mass transfer in MHD non-Darcian flow of a micropolar fluid over a stretching sheet embedded in a porous media with non-uniform heat source and thermal radiation," Communications in Nonlinear Science and Numerical Simulation, vol. 15, no. 7, pp. 1843–1857, 2010.

[21] Ali J. Chamkha, S.M.M. EL-Kabeir, A.M. Rashad (2013), Coupled heat and mass transfer by MHD natural convection of micropolar fluid about a truncated cone in the presence of radiation and chemical reaction, Journal of Naval Architecture and Marine Engineering, Vol. 10 (2), pp 158 – 168.

[22] M.A Seddeek., A.A Darwish, and M.S Abdelmeguid, (2007). Effects of chemical reaction and variable viscosity on hydromagnetic mixed convection heat and mass transfer for Hiemenz flow through porous media with radiation, *Commun Nonlinear Sci. Numer. simulat.*, 15, 195-213.

[23] A.M Salem, and M. Abd El-Aziz, (2008). Effect of Hall currents and chemical reaction on hydromagnetic flow of a stretching vertical surface with internal heat generation/absorption. *Applied Mathematical Modelling*, 32, 1236-1254.

[24] R.A Mohamed, (2009). Double-Diffusive Convection-radiation Interaction on Unsteady MHD Flow over a Vertical Moving Porous Plate with Heat Generation and Soret Effects, *Applied Mathematical Sciences*, 3, (13), 629-651.

[25] F.S Ibrahim., A.M Elaiw, and A.A Bakr, (2008). Effect of chemical reaction and radiation absorption on the unsteady MHD free convection flow past a semi infinite vertical permeable moving plate with heat source and suction. *Commun Nonlinear Sci. Numer. simulat.*, 13, 1056-1066.

[26] K. Vajravelu, and D. Rollins, (1992), Heat transfer in electrically conducting fluid over a stretching sheet, Int. J. Non-linear Mech., Vol.27, pp.265–277.

[27] A.A M Mostafa. and E. W. Shimaa, (2012), MHD flow and heat transfer of a micropolar fluid over a stretching surface with heat generation (absorption) and slip velocity, Journal of the Egyptian Mathematical Society, Vol.20, pp.20–27.

[28] R.N Jat, S. Vishal Saxena and Dinesh Rajotia, (2013), MHD flow and heat transfer near the stagnation point of a micropolar fluid over a stretching surface with heat generation/absorption, Indian Journal of Pure and Applied Physics, Vol.51, pp.683-689.

[29] E. M. Abo-Eldahab and M. A. El Aziz, "Flow and heat transfer in a micropolar fluid past a stretching surface embedded in a non-Darcian porous medium with uniform free stream," *Applied Mathematics and Computation*, vol. 162, no. 2, pp. 881–899, 2005.

[30] S Mohammed Ibrahim., T Sankar Reddy and N Bhaskar Reddy (2013), Radiation and mass transfer effects on MHD free convection flow of a micropolar fluid past a stretching surface embedded in a non-Darcian porous medium with heat generation, ISRN Thermodynamics, Volume 2013, Article ID 534750, pages 15.

[31] M.M Rahman, (2009), Convective flows of micropolar fluids from radiate isothermal porous surfaces with viscous dissipation and joule heating, Comm Nonlinear Sci Numer Simulat., Vol.14, pp.3018-3030.
[32] M.S Abel., K.A Kumar, and R Ravikumara, (2011), MHD flow, and heat transfer with effects of buoyancy, viscous and Joules dissipation over a nonlinear vertical stretching porous sheet with partial slip, Engineering, Vol.3, pp.285-291.
[33] K.L Hsiao, and B Lee, (2010), Conjugate heat and mass transfer for MHD mixed convection with viscous dissipation and radiation effect for viscoelastic fluid past a stretching sheet, World Academy of Science, Engineering and Technology, Vol.62, pp.318-325.
[34] B Gebhart, (1962), Effect of viscous dissipation in natural convection, J.Fluid Mech., Vol. 1, pp. 225- 232.
[35] K Govardhan, N Kisha, and M Chenna Krishna Reddy, (2011), Radiation Effect on MHD Steady Free Convection Flow of a Gas at a Stretching Surface with a Uniform Free Stream with Viscous Dissipation, Thammasat Int. J. Sc. Tech., Vol. 16, No. 2, pp.1-10.
[36] A.M Salem (2013), The Effects of Variable Viscosity, Viscous Dissipation and Chemical Reaction on Heat and Mass Transfer Flow of MHD Micropolar Fluid along a Permeable Stretching Sheet in a Non-Darcian Porous Medium, Mathematical Problems in Engineering Volume 2013 (2013), Article ID 185074, 10 pages
[37] M.A.A Mahmoud, (2009), Heat generation/absorption and viscous dissipation effects on MHD flow of a micropolar fluid over a moving permeable surface embedded in a non-darcian porous medium, JKPS, Vol.54, pp.1526–1531.
[38] A.J Willson (1970), Boundary layer in micropolar liquids, Mathematical Proceeding of the Cambridge Philosophical Society, Vol.67(2),pp.469-476.
[39] D.A Nield and A. Bejan (1999), convection in porous media, Springer, Newyork.
[40] M.Q Brewster (1992), Thermal radiative Transfer and properties, John Wiley and Sons, New York.